Mossbauer Effect in ^{57}Fe at 14keV

Bhaskar Mookerji and Charles Herder
MIT Department of Physics
(Dated: May 13, 2008)

We study the 14.4keV transition in ^{57}Fe using the recoilless emission of γ-rays from 270-day ^{57}Co embedded in a platinum substrate. The natural life time of the 14.4keV transition is measured to 95± 15ns by characterizing the line broadening of $Na_3Fe(CN)_6{\cdot}H_2O$ absorbers. The second-order Doppler shift coefficient $\kappa = -3k_B/2mc^2$ is determined to be $-(2.2 \pm 0.4) \times 10^{-15}$J/K. Various parameters of nuclear hyperfine structure: internal magnetization, isomer shifts, Zeeman and quadrapole splitting, and first excited and ground states of ^{57}Fe in metallic iron, Fe_2O_3, and Fe_3O_4 are determined, and a study of magnetization polarization suggests that metallic iron is preferentially polarized over its oxides. Accounting for possible oxide contamination, this suggestion is inconclusive.

Relative to traditional optical photon spectroscopy, nuclear γ-rays in the range of $10-100$keV possess a significantly higher spectroscopic resolving power on the order of their natural line width $\left(\Delta\nu/\nu \approx 10^{-12}\right)$. Such resolution has been important in studying nuclear and magnetic properties historically out of reach, particularly the ferromagnetism of iron and its compounds.

First, we will describe how the Mossbauer effect achieves resolution at the natural line width of γ-ray decay, and the characteristics of the resulting spectra. Of particular interest are the nuclear magnetic properties of metallic iron and various isomer shifts from alterations of its chemical oxidation state.

1. MOSSBAUER SPECTROSCOPY

Mossbauer spectroscopy resolves two obstacles to high-resolution γ-ray spectroscopy by embedding an emitting nucleus in a solid lattice. The first being the displacement of the emission line from absorption line by the recoil of the emitting nucleus; and the second being the Doppler broadening of effective line width from thermal motion.

From momentum conservation, an emitting nucleus receives a recoil energy R from a γ-ray given by

$$R = E_\gamma^2/2mc^2 \tag{1}$$

where E_γ is the γ-ray energy and m is the mass of the emitting nucleus. In this process, the probability for a transition in which the nucleus decays from an excited state N_i to a ground state N_f, and the lattice goes from an initial state L_i to a final state L_f is described by Fermi's Golden Rule:

$$\begin{aligned} P\left(N_i \to N_f, L_i \to L_f\right) &\propto \left|\left\langle f\right| H_{\text{int}} \left|i\right\rangle\right|^2 \\ &= \left|\left\langle L_f\right| e^{i\mathbf{k}\cdot\mathbf{r}} \left|L_i\right\rangle \left\langle N\right\rangle\right|^2, \end{aligned} \tag{2}$$

where H_{int} is the internal decay Hamiltonian, $\mathbf{k}$ is the wavevector of the emitted γ-ray and $\mathbf{r}$ is the center-of-momentum (c.m.) coordinate of the nucleus[1]. The independence of the nuclear properties from the crystal c.m. allows us to factor the nuclear matrix element $\langle N\rangle$ from that describing γ-ray momentum transfer to the lattice. The fraction of emitted or absorbed γ-rays without energy loss to the atom is given by the lattice element

$$f = \left|\left\langle L_i\right| e^{i\mathbf{k}\cdot\mathbf{r}} \left|L_i\right\rangle\right|^2. \tag{3}$$

Note that when ppproximating the lattice ground state as a harmonic oscillator with frequency ω, the fraction of emissions is $e^{-R/\hbar\omega}$, suggesting that Mossbauer emission occurs with high probability when $R \ll \hbar\omega$. For a general treatment as a solid lattice, the fraction of emissions is $e^{-k\langle x\rangle^2}$, where $\langle x\rangle^2$ is the mean-square deviation of a vibrating atom about its equilibrium position[1]. Therefore, within some Gaussian uncertainty, its state will remain unchanged following γ-ray emission.

A perturbative expansion of Equation 2 determines the natural line width resolving power. The probability that an emitted γ-ray will have an energy E is given by

$$\begin{aligned} P\left(E\right) &= \frac{\Gamma}{2\pi} \sum_{i,f} \frac{p_i \left|\left\langle i\right| e^{-i\mathbf{k}\cdot\mathbf{r}} \left|f\right\rangle\right|^2}{\left(E - E_0 + \epsilon_f - \epsilon_i\right)^2 + \frac{1}{4}\Gamma^2} \\ &\approx \frac{\Gamma/2\pi}{\left(E - E_0\right)^2 + \frac{1}{4}\Gamma^2} \end{aligned} \tag{4}$$

$|i\rangle$ and $|f\rangle$ are the initial and final states of the lattice, with energies ϵ_i and ϵ_f respectively[2]; and E_0 and Γ are the energy and width of the first excited state of the nucleus. Ultimately, the recoil energy and Doppler broadening for γ-rays are a function of the mass and thermal motion of the solid lattice, and are therefore completely negligible. *On average*, this energy transferred to the lattice just free recoil energy R[1]. The resulting emission has essentially energy and line width of the nuclear decay. Lastly, an emitting crystal moving with velocity v in the laboratory reference frame experiences a doppler shift from the emission energy E_0,

$$\frac{\Delta E}{E_0} = \frac{v}{c} = \beta, \tag{5}$$

allowing us to sweep through resonance absorptions.

---

[1] The change of state in a solid lattice by a nuclear gamma ray is describe by *Lipkin's sum rule*. See [3].

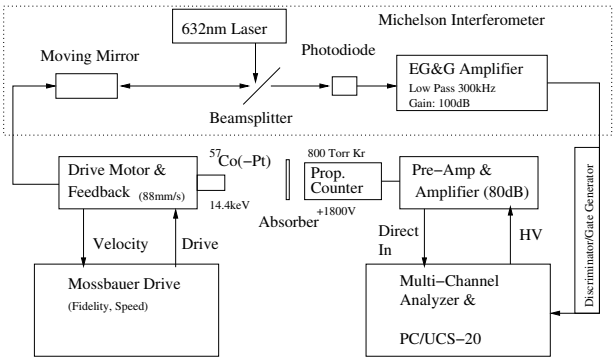

FIG. 1: Mossbauer scattering apparatus and Michelson interferometer.

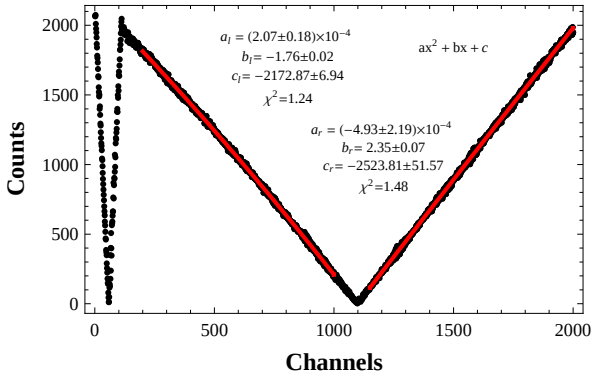

FIG. 2: Michelson interferometer velocity calibration.

1.1. Hyperfine Structure

The energy E_n of a hyperfine state in our spectra is given by

$$E_n = -g_n \mu_N I H + \frac{1}{2}\epsilon + \delta_n \tag{6}$$

where μ_N is the Bohr magneton, H is the effective magnetic field seen by the nucleus, and I is the nuclear spin. The first term is the nuclear Zeeman splitting which splits the excited ($I = 3/2$) and ground ($I = 1/2$) states into six energy levels with allowed Mossbauer transitions governed by selection rules $\Delta m = 0, \pm 1$. The second term ϵ is an electric quadrapole term present in samples with asymmetric electric charge distributions ($I > 1/2$).

The remaining term is known as the isomer shift and is observed when the emission source and absorption sample differ in chemical composition. Specifically, the s-electron density for both sources have a finite probability of being at the nucleus, thereby affecting the nuclear level structure. Assuming a finite-sized nucleus with ground and excited states $|g\rangle$ and $|e\rangle$, we can measure the difference in s-electron density at the nucleus between the emission source and absorption sample. The velocity with which the source must be moved toward the absorber to restore resonance is given by the isomer shift[2]:

$$\begin{aligned} \delta &= \Delta E_A - \Delta E_S \\ &\propto \left(\langle R_e^2\rangle - \langle R_g^2\rangle\right)\left(|\psi_s(0)|_A^2 - |\psi_s(0)|_S^2\right). \end{aligned} \tag{7}$$

We can equate transitions in the observed Mossbauer spectra to Equation 6 and then use a linear least squares method to determine the nuclear magnetic and chemical properties of ^{57}Fe and its compounds.

2. EXPERIMENTAL SETUP, PROCEDURE, AND CALIBRATION

The experimental apparatus we used to obtain Mossbauer spectra is shown in Figure 2. A proportional gas counter and measurement chain bin absorption events from recoil-free 14.4keV γ-rays sourced from 10mC 270-day ^{57}Co (embedded in Pt) undergoing beta decay to an excited ^{57}Fe nucleus. A single channel analyzer is used to discriminate the 14.4keV emission from other radiation not absorbed by ^{57}Fe. The source is mounted to a piston on a high-precision linear motor being driven by a periodic sawtooth waveform at a constant acceleration in both directions. The Doppler shifted photons traverse a variety of absorbers (metallic ^{57}Fe, $Na_3Fe(CN)_6{\cdot}H_2O$, Fe_2O_3, and Fe_3O_4) from whose Mossbauer absorption spectra we determine temperature and thickness parameter dependence, and other nuclear magnetic properties described in Equation 6.

A Michelson interferometer is coupled to the drive mechanism on the Mossbauer source to determine the fractional energy shift and velocity described by Equation 5. The interferometer consists of two paths, one fixed and the other oscillating, that register an interference pattern that can be discriminated and counted into bins corresponding to the velocity spectrum. The calibration data from our Michelson interferometer is given in Figure 2 and the velocity v_i of a given bin is related to the counts C_i by

$$v_i = C_i \lambda / 2NT, \tag{8}$$

where N is the total number of sweeps, T is the dwell time per bin, and λ is the wavelength of our interferometer (632nm HeNe).

3. RESULTS AND ERROR ANALYSIS

Mossbauer spectra were collected for a variety of samples previously described. Using the velocity calibration described in the previous section, we determined a secondary calibration spectrum from ^{57}Fe as a function of velocity as shown in Figure 3.1 A sample fit with Poisson counting error for a given absorption is well-described by a Lorentzian distribution with constant offset as seen in

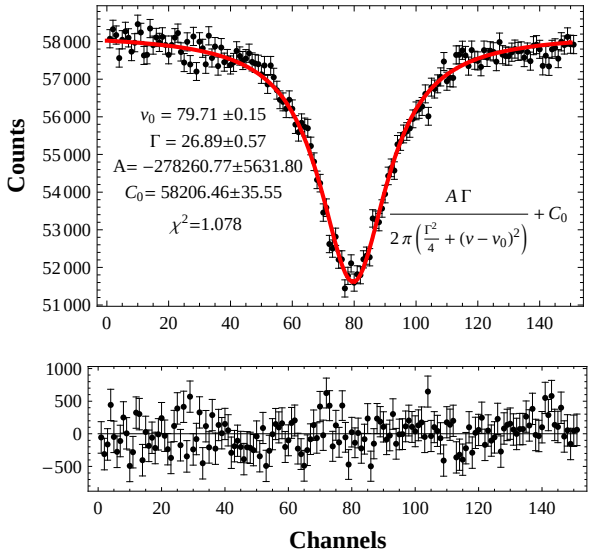

FIG. 3: Sample mossbauer absorption in Fe_2O_3 and residuals.

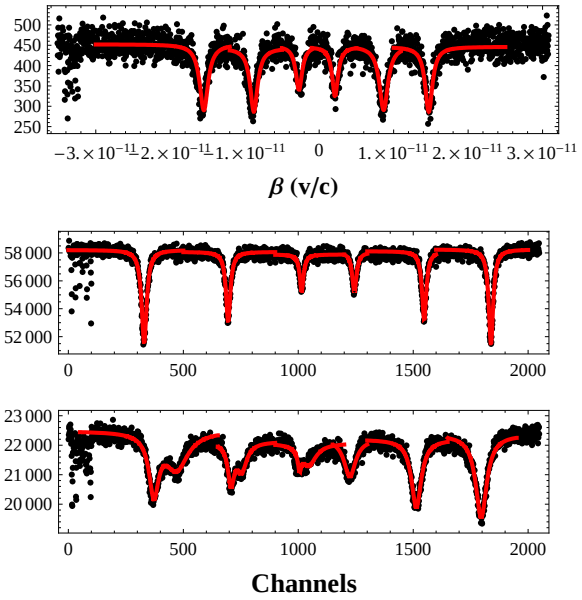

FIG. 4: Mossbauer spectra for ^{57}Fe, Fe_2O_3, and Fe_3O_4

Figure 3: residuals are randomly distributed and the fit applies with an excellent χ^2. In the following, we will see that the finite thickness of the absorber introduces Gaussian line broadening.

3.1. Thermal Time Dilation and Absorber Thickness

A second-order Doppler effect from thermal motion and the finite thickness of our absorbers are two relevant parameters for characterization in our absorption spectra. Time dilation arises from the thermal motions of the emitting and absorbing nuclei, and the mean square velocity $\overline{\langle v^2 \rangle}$ of the nucleus oscillating in the lattice increases with increased thermal motion. The observed frequency of a γ-ray emitted with respect to the lab frame at an angle θ_{lab} and velocity β is Doppler shifted by

$$\omega_{\text{lab}} = \omega_0 \frac{\left(1-\beta^2\right)^{1/2}}{1-\beta\cos\theta_{\text{lab}}}. \tag{9}$$

The second-order term of the ω_{lab} Taylor expanded is observable at the resolution of our experiment, and can be related (at thermal equilibrium) to temperature to yield the fractional shift:

$$\frac{\Delta E}{E_0} = -\frac{1}{2}\beta^2 = -\frac{3k_BT}{2mc^2}, \tag{10}$$

where m is the mass of the emitting atom and the constant of proportionality $\kappa = -3k_B/2mc^2$ is -2.41×10^{-15}J/K.

To determine this coefficient, we measured the center velocity of a stainless steel absorption as a function of temperature (22°C, 50°C, 120°C, and 180°C) in order to characterize the relative energy shift between the emitting source and the absorber. We reduced the speed of the Mossbauer drive to observe fractional changes, and found that a proportionality constant $-(2.2 \pm 0.4) \times 10^{-15}$J/K ($\chi^2 = 0.02$) within 1σ of the accepted value described earlier[4].

For absorption we also characterized the effects of finite absorber thickness by measuring the absorption line width of varying thicknesses of $Na_3Fe(CN)_6{\cdot}H_2O$ (0.1, 0.25, and 0.5g/mm^2). The cyanide anions and electrons are arranged symmetrically, eliminating any quadrapole and Zeeman splitting. The probability of a γ-ray being attenuated by the absorber increases exponentially through the sample, and so we can relate related linewidth against absorber thickness and extrapolate to zero thickness the natural line width of the 14.4keV transition in ^{57}Fe. Our measured linewidth $\Gamma_0 = 0.20 \pm 0.0124$mm/s is within 1σ of the published 0.19mm/s. The half-life of the 14.4keV transition is then $\tau_{1/2} = \hbar \ln 2/\Gamma_0 = 95 \pm 15$ns ($\chi^2 = 0.8$), also within 1σ of the published 97 ± 9ns[4].

3.2. Hyperfine Structure of Iron Compounds

Using ^{57}Fe as a secondary calibration source, we related Mossbauer transitions for Fe_2O_3 and Fe_3O_4 to Equation 6 and measured magnetic and chemical parameters given in Table I using a linear least squares method. A sample line width fit is given in Figure 3, and the overall Mossbauer spectra for metallic iron and its compounds are given in Figure 3.1. Following conventions in the reference literature, we present values in velocity units [mm/s] for g-factors $g_n' = g_n \mu_N H$.

TABLE I: Properties of iron Mossbauer absorbers[a] at 298K.

	^{57}Fe		Fe_2O_3		Fe_3O_4 (Tetrahedral)		Fe_3O_4 (Octahedral)	
	Measured	Published	Measured	Published	Measured	Published	Measured	Published
g_0'[mm/s]	3.3 ± 0.5	3.96 ± 0.1	6.17 ± 0.02	6.11 ± 0.05	6.26 ± 0.08	5.90 ± 0.2	5.81 ± 0.09	5.3 ± 0.2
g_1'[mm/s]	1.9 ± 0.25	2.23 ± 0.03	3.37 ± 0.04	3.45 ± 0.03	3.20 ± 0.10	3.35 ± 0.15	3.02 ± 0.07	3.1 ± 0.1
μ_1/μ_0[mm/s]	1.73 ± 0.4	1.69 ± 0.05	1.64 ± 0.02	1.69 ± 0.02	1.53 ± 0.04	1.7 ± 0.1	1.56 ± 0.03	1.75 ± 0.09
δ[mm/s]	0.08 ± 0.04	—	0.38 ± 0.05	0.47 ± 0.03	0.36 ± 0.09	0.45 ± 0.1	0.58 ± 0.10	0.7 ± 0.1
ϵ[mm/s]	—	—	0.124 ± 0.003	0.12 ± 0.03	0.16 ± 0.05	0.0 ± 0.1	0.03 ± 0.01	0.0 ± 0.1
$H_{\text{eff.}}$ [T]	$30. \pm 4$	33.0 ± 0.2	53.5 ± 0.6	51.5	52.4 ± 0.5	50 ± 2	47.0 ± 0.6	45 ± 2
θ [rad]	$\sim \pi/2$	$\pi/2$	Unpolarized	—	Unpolarized	—	Unpolarized	—

[a]See [4], [5], and [6].

Differences in these spectra elucidate the bonding geometry and oxidatation state of the ^{57}Fe. The *d*-electrons of metallic ^{57}Fe allow bonding in a lattice with cubic symmetry, thereby eliminating any charge asymmetry about the iron nucleus giving rise to quadrapole splitting in Mossbauer spectra. Our ^{57}Fe absorption sample differs slightly from our emitting source and has a measurable isomer shift. The ^{57}Fe spectrum is also symmetric about $\beta = 0$, whereas Fe_2O_3 and Fe_3O_4 are systematically offset by a isomer shift in *s*-electron density. Nuclear Zeeman and quadrapole splitting appear simultaneously in both Fe_2O_3 and Fe_3O_4: the four center absorptions are very slightly offset towards higher values, while the two outer absorptions are offset towards lower values. This offset corresponds to electrical quadrapole splitting. Widely-spaced Zeeman absorptions in both Fe_2O_3 and Fe_3O_4 correspond to greater magnetization $H_{\text{eff.}}$ at the iron nucleus.

The angle of polarization θ of magnetization $H_{\text{eff.}}$ is measured with respect to the direction of γ-ray emission and can, in theory, be determined from the relative peak intensities of the absorptions[4]. Emitted radiation is largely magnetic-dipole in character, and emission intensities are a function of a dipole distribution such that spectral peak intensities are $3 : \beta : 1 : 1 : \beta : 3$, where

$$\beta = \frac{4\sin^2\theta}{1+\cos^2\theta}. \tag{11}$$

At $\theta = \pi/2$, the intensity is 3:4:1:1:4:3 with linear polarizations, $\|:\perp:\|:\|:\perp:\|$. If the magnetizations are randomly oriented, then the emitted radiation is unpolarized and the intensities are 3:2:1:1:2:3 after averaging over all angles θ. A cursory glance at Figure 3.1, suggests that the internal magnetization is unpolarized in iron oxides, and possibly linearly polarized at $\theta = \pi/2$ for metallic iron. The inner peaks, however, clearly exceed the required intensity, suggesting that the absorption peaks are saturated due to the finite thickness of the absorber.

This polarization discrepancy is also partially explained by sample contamination, as in the case of Fe_3O_4. The Fe_3O_4 absorptions in Figure 3.1 are a composite of two different oxidation states for ^{57}Fe described by an *inverse spinel* group structure: $Fe_2^{+3}Fe^{+2}O_4$[6]. The solid is composed of unit cells of Fe^{+3} and Fe^{+2} bonded as tetrahedral and octrahedral oxides. Because the nuclear magnetic moment $\mu_{Fe^{+3}}$ is greater than $\mu_{Fe^{+2}}$, the outer doublets in the Fe_3O_4 absorption spectra correspond to Fe^{+3}, which produces a larger magnetization. While the ferric and ferrous ions in the octahedral sites of Fe_3O_4 produce their own unique magnetic fields at the iron nuclei, the split peak heights for the octahedral and tetrahedral oxides do not have a 2:1 stoichiometric ratio, suggesting the an alteration or contamination of the sample with some other iron oxide.

4. CONCLUSIONS

Despite the perils of oxide contamination and absorption saturation, high intrinsic resolution makes Mossbauer spectroscopy particular fascinating for investigating magnetization properties of ferromagnetic materials. In the future, particularly ambitious 8.14 students might contemplate studies of magnetization dependence on temperature.

[1] H. Frauenfelder, *The Mossbauer Effect: A Review—with Collection of Preprints* (W.A. Benjamin, Inc., 1962).
[2] A. Boyle and H. Hall, Reports on Prog. Phys. pp. 441–524 (1962).
[3] H. Lipkin, Annals of Physics **9**, 332 (1960).
[4] S. H. R.S. Preston and J. Heberle, Phys. Rev. pp. 2207–2218 (1962).
[5] O. Kirstner and A. Sunyar, Phys. Rev. Lett. pp. 412–415 (1960).
[6] A. M. S. O. R. Bauminger, S.G. Cohen and E. Segal, Phys. Rev. Lett. pp. 1447–1450 (1961).